J Supercond Nov Magn (2011) 24:1665–1672
DOI 10.1007/s10948-010-1081-5

ORIGINAL PAPER

# Griffiths Phase and Disorder in Perovskite Manganite Oxides $La_{1-x}Ca_xMnO_3$ and $La_{0.7}Sr_{0.3}MnO_3$

**Hongguang Zhang · Lingshan Chen · Yongtao Li · Hao Liu · Yuanyuan Chen · Kai Chen · Xueguang Dong · Hao Yang · Tianyou Gao · Qi Li**

Received: 9 September 2010 / Accepted: 29 November 2010 / Published online: 30 December 2010


**Abstract** Polycrystalline samples $La_{1-x}Ca_xMnO_3$ ($x = 0.17, 0.15, 0.10$) and $La_{0.7}Sr_{0.3}MnO_3$ were prepared in order to investigate the Griffiths-like features induced by disorder compared with their counterpart single crystals. The magnetization data exhibit the traditional transition from ferromagnetic phase to paramagnetic phase. From the temperature dependence of inverse susceptibility, it can be testified that the Griffiths-like features still exist in as-prepared Ca doped samples, while non-Griffiths-like features exist in $La_{0.7}Sr_{0.3}MnO_3$. All these samples, however, exhibit the large effective spins resulting from formation of the short-order ferromagnetic clusters. The O $K$-edge X-ray absorption spectra indicate the Jahn–Teller (J-T) distortions are definitely present due to the J-T ion $Mn^{3+}$, which indicate that static J-T distortion is not a sufficient condition for the existence of Griffiths phase in Sr-doped system. And, the size of J-T distortion is a little larger in polycrystalline $La_{0.7}Sr_{0.3}MnO_3$ than that in polycrystalline samples $La_{1-x}Ca_xMnO_3$ ($x = 0.17, 0.15, 0.10$), revealed by X-ray diffraction parameters and extended X-ray fine structure absorption data of Mn $K$-edge. It also testifies that the disorder in $La_{0.7}Sr_{0.3}MnO_3$ caused by both chemical doping and J-T distortions is lower than that in polycrystalline samples $La_{1-x}Ca_xMnO_3$, which may be the reason of non-Griffiths-like phase existing in $La_{0.7}Sr_{0.3}MnO_3$ samples.

H. Zhang · L. Chen · Y. Li · H. Liu · Y. Chen · K. Chen · X. Dong · H. Yang · T. Gao · Q. Li (✉)
Physics Department, Southeast University, Nanjing, 211189, P.R. China
e-mail: qli@seu.edu.cn

Y. Li
College of Science, Nanjing University of Posts & Telecommunications, Nanjing, 210046, P.R. China

**Keywords** Griffiths phase · Manganite oxides · Disorder · Jahn–Teller (J-T) distortions · XAFS

## 1 Introduction

Perovskite manganite oxides with many various physical features have been investigated for a long time. $La_{1-x}Ca_xMnO_3$ [1–3] and $La_{1-x}Sr_xMnO_3$ [4, 5] are reckoned as two prototypical systems. Since the colossal magnetoresistance (CMR) effect has been found in ceramic material $La_{1-x}Ca_xMnO_3$ by Jin et al. [6] in 1994, the CMR effect has been becoming a leading and important issue to researchers. Many kinds of models and statements have been proposed to explain CMR effect, such as double exchange (DE) [7] interaction, Jahn–Teller (J-T) effect [8], polaron model [9], but non-agreements have been reached. Recently, theoretical calculation has found that CMR effect is caused by intrinsic inhomogeneous [10]. A new temperature scale $T^*$ where clusters start forming well above the Curie temperature is noted. Burgy et al. [10] regarded this temperature as Griffiths temperature. More experiments have testified the existence of Griffiths phase in perovskite manganites through A-site doping [11–15]. In 2002, Salamon proposed that CMR is a Griffiths singularity [11]. However, non-Griffiths-like phase has been observed in this system, which still has CMR effect [16]. Moreover, more samples with non-Griffiths-like phase are observed in CMR materials these days [16–18]. Therefore, whether the Griffiths phase is the prerequisite for CMR needs to be further validated.

In order to understand the non-Griffiths-like phase in $La_{1-x}Ca_xMnO_3$ and $La_{1-x}Sr_xMnO_3$ systems, it is necessary to overview their complex phase diagrams as a function of temperature and chemical concentration ($x$). For $La_{1-x}Ca_xMnO_3$ [1], it exhibits a canted-antiferromagnetic

insulating (CI) state when concentration $x$ below 0.125. As the doping level increases to $0.125 \leq x \leq 0.18$, it evolves into a ferromagnetic insulating (FI) state. Ferromagnetic metallic (FM) state appears along with a higher doping level $0.22 \leq x \leq 0.50$. In this region, the CMR effect exists and GP-like feature shows ($x < 0.33$). However, in [19], GP-like features were also observed even for the calcium concentration $x$ across the compositional metal-insulator boundary. Both of single crystals $La_{0.82}Ca_{0.18}MnO_3$ and $La_{0.80}Ca_{0.20}MnO_3$ show non-GP-like features. Meanwhile, $La_{1-x}Sr_xMnO_3$ system [20] displays a CI state in the range of $0 \leq x < 0.1$. The phase becomes an FI state as the doping level increases to $0.1 \leq x \leq 0.15$ and an FM state in the range of $0.15 < x \leq 0.5$. Interestingly, the concentration scope of GP ($0.06 < x < 0.16$) in this system is totally different from that in Calcium-doped system. That is, GP feature mainly exists in the range of FM state for Ca-doped system, while it mostly occurs in the FI state for Sr-doped system. This kind of divergence between those two systems is unclear now. Consequently, to investigate the situation of GP in non-GP doping range for corresponding polycrystalline samples can make a further understanding to the different mechanisms of those two systems.

The presence of GP-like features was discussed by Griffiths [21–23] originally. The formation of GP-like features is induced by intrinsic inhomogeneities [24], which are caused by quenched disorder by A-site cation doping. Perovskite manganite oxides are intrinsically disordered because of local lattice distortion caused by both the mismatch of A-site cation size and the J-T effect. Thus, disorders in the systems play an important role in the formation of GP. As is known, the lattice structure in polycrystalline sample is definitely much more disordered than that in single crystal of same system. Therefore, compared with single crystal, the GP-like features must be enhanced by the higher degree of disorder in polycrystalline samples, which is proved in Ref. [25]. And the temperature ranges of GP-like features in polycrystalline $La_{0.8}Ca_{0.2}MnO_3$ and $La_{0.79}Ca_{0.21}MnO_3$ compounds are exactly extended relative to those in single crystals of the same samples. In addition, the disorder source of GP existence has not been totally understood. The formation of GP-like features in $La_{1-x}Ca_xMnO_3$ system is caused by the disorder arising from the Mn–O–Mn bond bending [11, 16, 26]. On the contrary, quenched disorder with static J-T distorted structure is the prerequisite for the observation of GP in $La_{1-x}Sr_xMnO_3$ system [12]. It can be deduced that this difference of disorder may cause different situations of GP induced by the higher degree of disorder of polycrystalline samples compared with the corresponding single crystals. Therefore, it is necessary to investigate the existence of GP and the situation of disorder in polycrystalline $La_{1-x}Sr_xMnO_3$ system in the doping range of non-GP in single crystals, compared with polycrystalline samples $La_{1-x}Ca_xMnO_3$.

Based on the statements above, polycrystalline $La_{0.7}Sr_{0.3}MnO_3$ is prepared for sake of detecting the GP phenomenon in this paper. In order to make sure the difference in the degree of disorder between Ca-doped and Sr-doped systems, polycrystalline $La_{1-x}Ca_xMnO_3$ ($x = 0.17$, 0.15, 0.10) are also synthesized for comparison with polycrystalline $La_{0.7}Sr_{0.3}MnO_3$ sample. It is found that there are differences in the formation of GP between the two systems from magnetization data.

## 2 Experimental Details

The polycrystalline specimens used in the present study, with nominal compositions $La_{1-x}Ca_xMnO_3$ ($x = 0.17$, 0.15, 0.10) and $La_{0.7}Sr_{0.3}MnO_3$, were prepared by sol-gel method and characterized by various techniques. The structure and phase purity of the specimens were checked by powder X-ray diffraction (XRD) using Cu-$K\alpha$ radiation at room temperature. The magnetization was measured by Quantum Design Physical Properties Measurement System (PPMS) with 100 Oe magnetic fields. The O $K$-edge X-ray absorption spectra (XAS) were measured at Beijing Synchrotron Radiation Facility. Extended X-ray absorption fine structure (EXAFS) spectra at Mn $K$ edge of our specimens were performed at room temperature at National Synchrotron Radiation Laboratory (NSRL), University of Science and Technology of China (USTC). For the analysis of EXAFS data using USTCXAFS2.0 code [27], the EXAFS oscillation signals were extracted after background subtraction and were normalized by fitting the pre-edge with New Victoreen method. And the $k^3$ weighted EXAFS oscillation signals were converted into $k$ space by Fourier transforms. The Fourier transforms of Mn $K$-edge were performed over the range of 2.6–12.7 $Å^{-1}$. The first shell oscillation signals were fitted with the amplitude reduction factor $S_0^2 = 0.75$ for as-prepared Ca-doped samples and $S_0^2 = 0.83$ for as-prepared Sr-doped sample using FEFF7.0 program.

## 3 Results and Discussions

XRD patterns of our samples are shown in Fig. 1. The XRD patterns show that all samples are in single phase and no obvious additional phases are found. As-prepared samples $La_{1-x}Ca_xMnO_3$ ($x = 0.17$, 0.15, 0.10) belong to orthorhombic $Pbnm$ structure ($O'$) and $La_{0.7}Sr_{0.3}MnO_3$ displays the rhombohedral structure ($R$), which is in agreement with the reported results [28, 29]. The disparate structural characteristic may have an important impact on the existence of GP-like features, which can be mentioned in later section. The corresponding lattice parameters, $a$, $b$, and $c$, which are fitted by least square and Bragg formula, are given

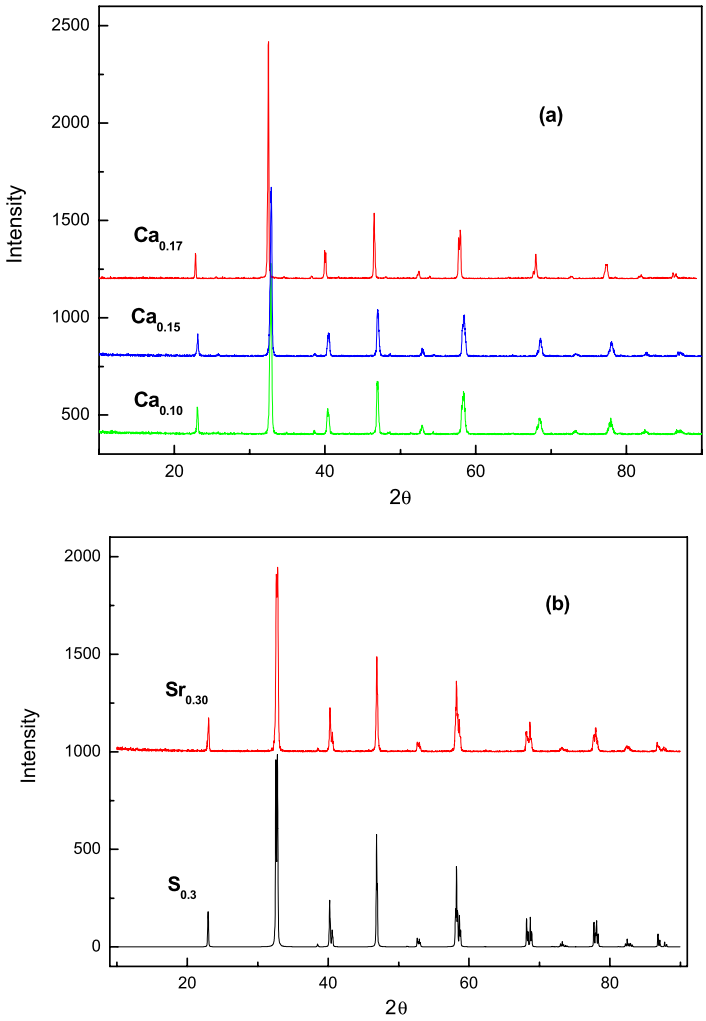


**Fig. 1** X-ray diffraction patterns of $La_{1-x}Ca_xMnO_3$ (**a**) and $La_{1-x}Sr_xMnO_3$ (**b**) samples. Making a contrast, the bottom curve ($S_{0.3}$) in (**b**) is the standard XRD pattern of $La_{0.7}Sr_{0.3}MnO_3$ which roots in an inorganic crystal structure database-NIST/FIZ [41]

**Table 1** Structure parameters fitted based on the first shell of XAFS and XRD patterns. ($\sigma$ is the disorder factor, $R$ is the fitted Mn–O band length, $a$, $b$, $c$ are the lattice parameters, $\triangle_{JT}$ represents the size of J-T distortion)

| Samples ($x$) | $\sigma$ | $R$ (nm) | $a$ (nm) | $b$ (nm) | $c$ (nm) | $\triangle_{JT}$ |
|---|---|---|---|---|---|---|
| $La_{0.9}Ca_{0.10}MnO_3$ | $0.078 \pm 0.005$ | 0.1926 | 0.5477 | 0.5470 | 0.5457 | 0.1099 |
| $La_{0.85}Ca_{0.15}MnO_3$ | $0.076 \pm 0.004$ | 0.1925 | 0.5481 | 0.5465 | 0.5438 | 0.1072 |
| $La_{0.83}Ca_{0.17}MnO_3$ | $0.076 \pm 0.003$ | 0.1917 | 0.5518 | 0.5531 | 0.5434 | 0.0845 |
| $La_{0.7}Sr_{0.30}MnO_3$ | $0.064 \pm 0.004$ | 0.1941 | 0.5490 | 0.5490 | 1.3325 | 0.1213 |

in Table 1. It shows that the lattice parameter $a$ decreases, while the lattice parameter $c$ increases with the increase of doped Ca concentration.

The temperature dependence of magnetization ($M(T)$) is shown in Fig. 2. All samples undergo a transition from FM phase to PM phase at the transition temperature ($T_C$) during heating from low temperature. The $T_C$ is defined as the temperature corresponding to the peak of $dM/dT$ in the $M(T)$ curve. The values of $T_C$ are given in Table 2, which is consistent with the values reported elsewhere [20, 30]. In Fig. 2(a), the values of $T_C$ shift to lower temperature with the decrease of Ca doping concentration, which is induced by the weakening of ferromagnetic DE interaction and the enhancing of anti-ferromagnetic superexchange interactions, as a consequence of the reduced $Mn^{4+}$ concentration, in this low doping concentration of the system. The temperature dependence of the inverse magnetic susceptibility is shown in Fig. 3. At high temperature range, the parts of PM were fitted by Curie–Weiss law, i.e.,

$$HM(0)/M(T) = \frac{3k_B T_C}{g\mu_B(S_{\text{eff}}+1)}\left(\frac{T}{T_C}-1\right)$$

where $S_{\text{eff}}$ is the effective spin, $g$ is the Lande factor, $\mu_B$ is the Bohr magneton, and $T_C$ is the Curie temperature. The relevant fitted parameters are given in Table 2. It can be seen clearly from Fig. 3(b) that the relation

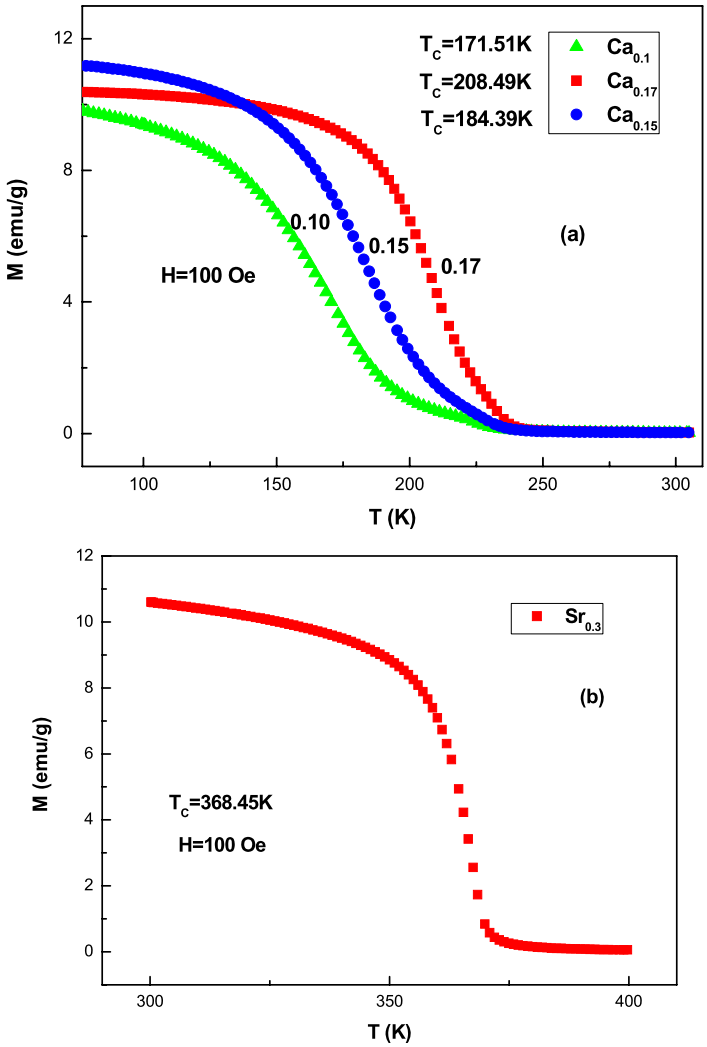


**Fig. 2** Temperature dependence of magnetization of $La_{1-x}Ca_xMnO_3$ ($x = 0.17$, 0.15, 0.10) samples (**a**), and $La_{0.7}Sr_{0.3}MnO_3$ (**b**). Magnetization measurements were performed for the samples on heating in a low field of 100 Oe after cooling in the field (FC)

**Table 2** Parameters fitted from magnetization curve. ($T_C$ is Curie temperature, $T_C^*$ is the Griffiths characteristic temperature, $S_{eff}$ is the effective spin fitted by Curie–Weiss law, $S_{eff}^*$ is the weighted value of $Mn^{3+}$ and $Mn^{4+}$, $\lambda$ is the exponent)

| Sample | $T_C$ (K) | $T_C^*$ (K) | $S_{eff}$ | $S_{eff}^*$ | $\lambda$ |
|---|---|---|---|---|---|
| $La_{0.9}Ca_{0.10}MnO_3$ | 171.51 | 227.31 | 5.18 | 1.950 | 0.255 |
| $La_{0.85}Ca_{0.15}MnO_3$ | 184.39 | 230.95 | 3.90 | 1.925 | 0.343 |
| $La_{0.83}Ca_{0.17}MnO_3$ | 208.49 | 235.15 | 4.24 | 1.915 | 0.398 |
| $La_{0.7}Sr_{0.30}MnO_3$ | 368.45 | – | 2.94 | 1.85 | – |

between inverse magnetic susceptibility ($H/M$) and temperature $T$ follows the Curie–Weiss law pretty well for $La_{0.7}Sr_{0.3}MnO_3$, whereas, for $La_{1-x}Ca_xMnO_3$ ($x = 0.17$, 0.15, 0.10), the Curie–Weiss law are not in accordance with the experimental curves in the full PM temperature range. That is because there are obviously sharp downturn in $H/M \sim T$ curves well above $T_C$, which is the characteristic [11] of Griffiths singularity. It means that the GP exists in as-prepared Ca doped polycrystalline system even for the concentration outside of the GP diagram [19] for single crystal $La_{1-x}Ca_xMnO_3$. The higher degree of disorder in polycrystalline samples than that in single crystal may be the reason of the existence of GP in as-prepared Ca doped polycrystalline samples. According to the reports [11, 16, 26] that the disorder arising from the bending of Mn–O–Mn bond induces the formation of GP-like features in $La_{1-x}Ca_xMnO_3$ system, it can be expected that the higher local disorder caused by polycrystalline samples may bend the Mn–O–Mn bond much stronger between some local areas. Thus, the GP turns up in the system. However, although the higher degree of disorder also exists in polycrystalline samples relative to the single crystal, the situation of obeying the Curie–Weiss law for $La_{0.7}Sr_{0.3}MnO_3$ signifies non-GP-like features observed, which is same as the reports [12] in corresponding single crystal. The region of Griffiths ($T$–$x$) phase diagram for $La_{1-x}Sr_xMnO_3$ ($0.06 < x < 0.16$) shapes a triangle [12], and the Griffiths characteristic temperatures are nearly same, that is, $T_C^* \sim 270$ K.

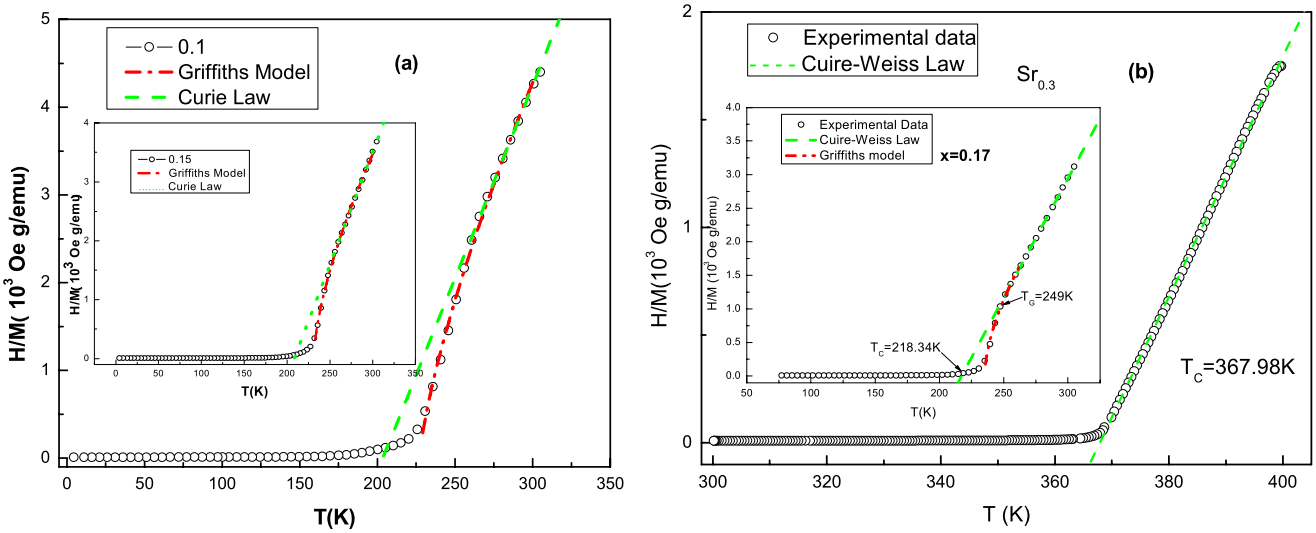


**Fig. 3** Temperature dependence of inverse magnetic susceptibility of $La_{0.9}Ca_{0.1}MnO_3$ sample (**a**), $La_{0.85}Ca_{0.15}MnO_3$ (*inset* (**a**)), $La_{0.7}Sr_{0.3}MnO_3$ (**b**), and $La_{0.83}Ca_{0.17}MnO_3$ (*inset* (**b**))

And it is also reported that the Curie temperature of as-prepared sample is 368.45 K, which is much higher than the upper limit of the GP temperature. The non-GP-like feature in polycrystalline sample $La_{0.7}Sr_{0.3}MnO_3$, therefore, is quite different from the status of GP in polycrystalline samples $La_{1-x}Ca_xMnO_3$. Thereupon, the GP-like feature is not observed for $La_{0.7}Sr_{0.3}MnO_3$ sample although the higher degree of disorder also exists in polycrystalline samples relative to the single crystal. As mentioned earlier, quenched disorder with static J-T distorted structure is the nature for the existence of GP in $La_{1-x}Sr_xMnO_3$ system [12]. Nevertheless for a non-GP feature in as-prepared sample $La_{0.7}Sr_{0.3}MnO_3$, that is because the static disorder is annealed [12] when the concentration $x$ greater than 0.16. And the structural phase comes into rhombohedral phase, which is in accordance with the experimental result from XRD pattern. Another reason is, as discussed by EXAFS in the below, the lower degree of disorder caused by chemical substitution and J-T distortion for as-prepared $La_{0.7}Sr_{0.3}MnO_3$ relative to as-prepared $La_{1-x}Ca_xMnO_3$.

Furthermore, the presence of GP-like features implies the FM clusters existing in the PM matrix. This can be testified by the large effective spin $S_{\text{eff}}$ [15, 25, 31]. According to the Curie–Weiss law, the effective spin $S_{\text{eff}}$ is fitted in Table 2. It can be seen that the values of $S_{\text{eff}}$ for $La_{1-x}Ca_xMnO_3$ ($x = 0.17$, 0.15, 0.10) are twice larger than the weighted average value of $S_{\text{Mn}}^{3+} = 2$ and $S_{\text{Mn}}^{4+} = 3/2$. However, the value of $S_{\text{eff}}$ for $La_{0.7}Sr_{0.3}MnO_3$ is not that much larger, just 2.94. Such a large value of $S_{\text{eff}}$ may indicate the appearance of magnetic cluster in PM region. And this behavior is attributable to ferromagnetic dimers [18, 32] which

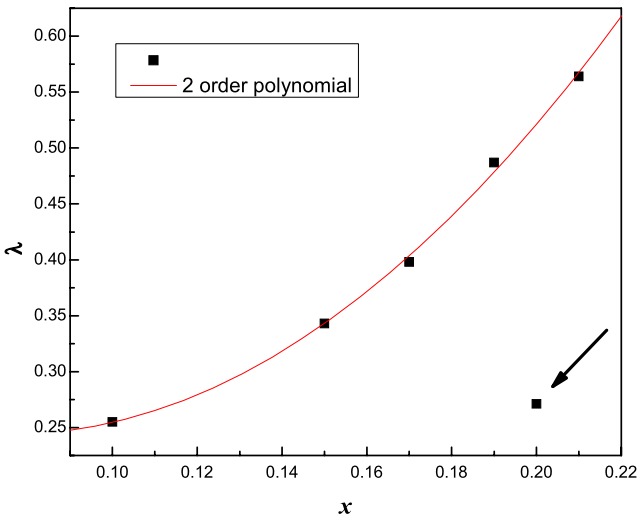


**Fig. 4** The relationship between exponent λ and concentration $x$

can be described by the coupling of free magnetic ions and pairs of Mn magnetic ions via DE interaction [33]. From the comparison of those data, it can be found that the existence of FM short range clusters is not the sufficient condition for the presence of GP, which has already been proposed in literature [34]. He et al. testified the formation of short-range order ferromagnetic clusters by neutron scattering and magnetometry data [34], but the fact that a phase separated state is distinct from GP demonstrates that Griffiths model is not universally applicable to complex oxide exhibiting performed ferromagnetic clusters. However, the occurrence of GP-like features in reverse can definitely give rise to the larger effective spin.

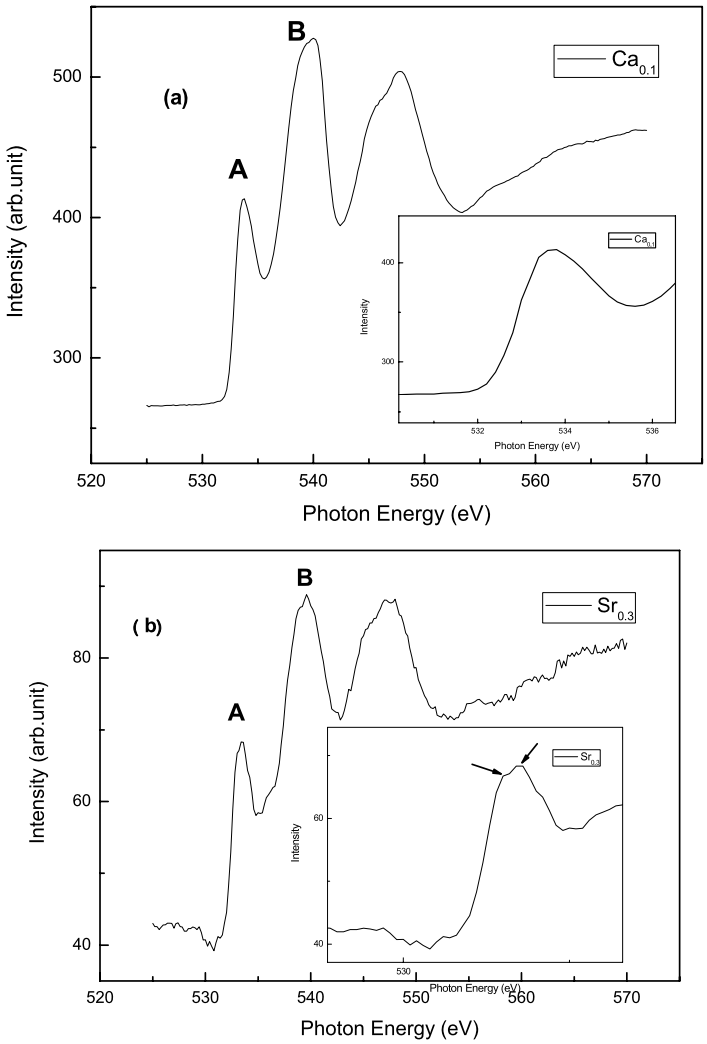


**Fig. 5** The O $K$-edge X-ray absorption spectra from as-prepared samples $La_{0.9}Ca_{0.1}MnO_3$ (**a**) and $La_{0.7}Sr_{0.3}MnO_3$ (**b**). The *insets* of both figures show the amplified parts of peak $A$

In Fig. 3, the dot-dash-line stands for the fitted results derived from Griffiths model, which can be expressed by power law prediction

$$\chi^{-1}(T) \propto (T - T_C^*)^{1-\lambda}, \tag{1}$$

where $0 < \lambda < 1$.

The exponent $\lambda$ and Griffiths characteristic temperature $T_C^*$ are deduced on the basis of (1), shown in Table 2. Combining with the data of exponent $\lambda$ in [25], the relationship between exponent $\lambda$ and concentration $x$ is shown in Fig. 4. Interestingly, the tendency of all points except $x = 0.20$ is satisfied with the parabolic relation. This reductive tendency can be explained by decreasing of the degree of disorder, which is proved by Debye–Waller factor $\sigma$ in the latter part.

In Fig. 5, the pre-edge structure of O $K$-edge XAS of all as-prepared samples at room temperature are shown in Fig. 5(a) for the as-prepared $La_{0.9}Ca_{0.1}MnO_3$ sample and Fig. 5(b) for the $La_{0.7}Sr_{0.3}MnO_3$ sample, respectively. The O $K$-edge absorption process is related with the O $1s$ to $2p$ dipole transition. The shapes of the two spectra are mainly the same [33]. The peak A is attributed to the mixing of the Mn 3d states with oxygen 2p states. XAS spectra of the O $K$-edge can indicate the presence of J-T distortions, since these spectra can reflect the strong hybridization of O $2p$ orbital with Mn $3d$ at nearly 533 eV. As reported, the presence or absence of doublet peaks [36] at nearly the photon energy point of Mn $3d$ is a signature for J-T distortions in the $MnO_6$ octahedra. From the inset of Fig. 5(a), it can be seen that there are no two separated peaks, which means the J-T distortions are fully developed above $T_C$. However, there is also dissimilarity in characteristic of the XAS spectra between Ca- and Sr-doped systems. In the inset of Fig. 5(b), the two distinct peaks separated by nearly 0.6 eV are found, which indicates the reduction of J-T distortions for $La_{0.7}Sr_{0.3}MnO_3$ sample. This result is consistent with the results in literatures [32, 33], which is interpreted as the separation of the $t_{2g}^{\downarrow}$ from the $e_g^{\uparrow}$ states. As is known to the conclusion in [37], no matter Ca- or Sr-doped systems, J-T distortions develop with increasing tempera-

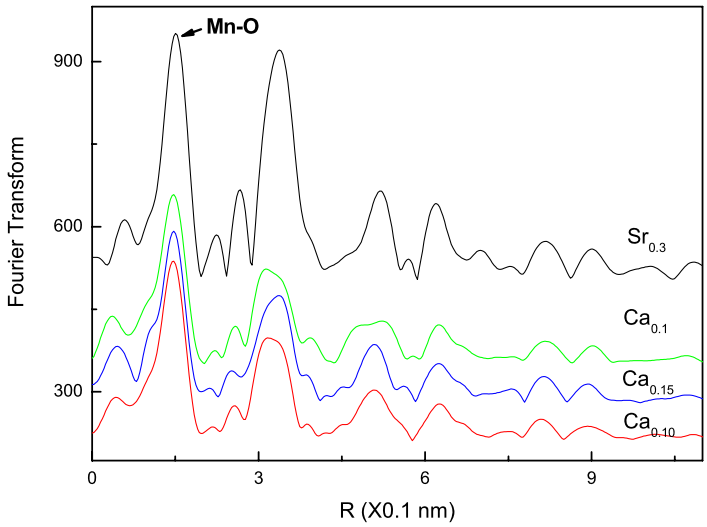


**Fig. 6** Fourier transforms of XAFS spectra of as-prepared samples at room temperature

ture and saturate once the systems come into PM states. Thus, the J-T distortions will be fully developed above $T_C$ in polycrystalline $La_{0.7}Sr_{0.3}MnO_3$, same as what is shown in Fig. 4(a). Therefore, the fully developed J-T distortion exists in both Ca- and Sr-doped systems in the PM region. And the size of J-T distortion ($\Delta_{JT}$) is calculated by lattice parameter from XRD patterns and the following XAFS data. The distribution of oxygen atom near Mn atom reveals three kinds of Mn–O band length. Two of them are intralayer Mn–O(1) band ($R_1$) and inter-layer Mn–O(2) band ($R_2$), respectively. The third of Mn–O(3) bands ($R_3$) is along the $a(b)$-axis [38]. The size of J-T distortion is defined as $\Delta_{JT} = (R_1 + R_2)/2R_3$ [39], and the values of which are shown in Table 1. It shows that the size of J-T distortion decreases in as-prepared Ca-doped system with the increase of Ca doped concentration because such doping weakens the J-T distortion due to the decrease of $Mn^{3+}$ concentration. As to as-prepared $La_{0.7}Sr_{0.3}MnO_3$ sample, the value of J-T distortion is a little larger than that of Ca-doped system. It indicates that static J-T distortion is not the sufficient condition for the existence of GP in $La_{1-x}Sr_xMnO_3$ system, due to the non-GP feature with J-T distortion in as-prepared polycrystalline sample $La_{0.7}Sr_{0.3}MnO_3$.

In order to investigate disorder of systems by clarifying the local structure near the central atom Mn, the Mn $K$-edge EXAFS spectra are detected using synchrotron radiation source. Figure 6 shows the Fourier transformed spectra of as-prepared samples. The intensity of various peaks indicates the information of corresponding coordination shells. The first peak (at ∼0.15 nm) with the highest intensity of all peaks represents the first coordination shell (Mn–O band), which contains several Mn–O band lengths, while the broad peak centered near 0.32 nm is a multipeak with contributions from Mn–(Ca/Sr), Mn–La, and Mn–Mn pairs. According to the first shell signal, the structure parameters are fitted by the least square with the coordination number $N$ fixed to 6 based on the single scattering theory [40], shown in Table 1. From Table 1, it can be seen that the average length of Mn–O band is decreasing with the increasing of doped Ca concentration. This tendency of average length of Mn–O band results from the size mismatch of A-site doped cation, i.e., the radius of $Ca^{2+}$ ion (0.099 nm) is smaller than that of $La^{3+}$ ion (0.106 nm). The disorder factor $\sigma$ (Debye–Waller Factor) is almost same for Ca-doped samples within the error range. The EXAFS experimental results show that the $MnO_6$ octahedron is distorted, which may be caused by the chemical doping and J-T distortion. Compared with the structure parameters of Ca-doped system, the smaller disorder factor of polycrystalline $La_{0.7}Sr_{0.3}MnO_3$ is shown in Table 1, which can mainly be attributed to the size mismatch of A-site cation because Sr-doping exhibits a little larger $\Delta_{JT}$ relative to Ca-doped system. It is known that the radius of $Sr^{2+}$ ion (0.112 nm) is closer to the $La^{3+}$ ion (0.106 nm) than $Ca^{2+}$ ion, thus the disorder caused by Sr doping will be smaller than that of Ca doping, which means the lower disorder factor in Sr-doped samples. Combined with the value of J-T distortion in Table 1, it can be seen that chemical doping plays a vital role in system disorder. And the degree of disorder caused by both chemical substitution and J-T distortion is smaller in as-prepared sample $La_{0.7}Sr_{0.3}MnO_3$ than that of as-prepared samples $La_{1-x}Ca_xMnO_3$ on the whole. Therefore, it can be easy to understand from the discussion above that the non-GP-like feature in polycrystalline $La_{0.7}Sr_{0.3}MnO_3$ is due to the lower degree of disorder caused by both chemical doping and J-T distortion.

## 4 Conclusions

In order to investigate the GP-like features induced by disorder, polycrystalline samples $La_{1-x}Ca_xMnO_3$ ($x = 0.17$,

0.15, 0.10) and $La_{0.7}Sr_{0.3}MnO_3$ were prepared. The magnetization data show the GP-like features still exist in as-prepared Ca doped samples, while non-GP-like features exist in $La_{0.7}Sr_{0.3}MnO_3$. The O $K$-edge XAS spectra indicate the J-T distortions are definitely present due to the J-T ion $Mn^{3+}$, which implies that static J-T distortion is not a sufficient condition for the existence of GP. However, the calculated size of J-T distortion by XRD and EXAFS data is a little larger in polycrystalline $La_{0.7}Sr_{0.3}MnO_3$ than that in polycrystalline samples $La_{1-x}Ca_xMnO_3$ ($x = 0.17$, 0.15, 0.10). It also testifies that the degree of disorder in $La_{0.7}Sr_{0.3}MnO_3$ caused by both chemical doping and J-T distortions is smaller than that in polycrystalline samples $La_{1-x}Ca_xMnO_3$.

**Acknowledgements** We are thankful to National Natural Scientific Fund of China for the project 10979016 and the innovation fund for graduate students, NSRL, USTC. Beijing Synchrotron Radiation Facility is also thanked for the beamtime we were offered for our measurements. We are also in debt to Yi Zhang, Southeast University, Zhi Xie, Bo He, Shiqiang Wei, Fengchun Hu, NSRL, USTC, and Haijie Qian, Ibrahim Kurash, BSRF, Institute of high-Energy physics, for their helps in XRD, magnetization, XAFS, and XAS measurements, respectively, and data process for XAFS as well.

## References

1. Schiffer, P., Ramirez, A.P., Bao, W., Cheong, S.-W.: Phys. Rev. Lett. **75**, 3336 (1995)
2. Coey, J.M.D., Viret, M., Molnar, S.V.: Adv. Phys. **48**, 167 (1999)
3. Hueso, L.E., Rivas, J., Rivadulla, F., López-Quintela, M.A.: J. Appl. Phys. **86**, 3881 (1999)
4. Moritomo, Y., Asamitsu, A., Tokura, Y.: Phys. Rev. B **51**, 16491 (1995)
5. Deisenhofer, J., Kochelaev, B.I., Shilova, E., Balbashow, A.M., Loidl, A., Krug von Nidda, H.-A.: Phys. Rev. B **68**, 214427 (2003)
6. Jin, S., Tiefei, T.H., McCormack, M., Fastnacht, R.A., Ramesh, R., Chen, L.H.: Science **264**, 413 (1994)
7. Zener, C.: Phys. Rev. **82**, 403 (1951)
8. Millis, A.J., Littlewood, P.B., Shraiman, B.I.: Phys. Rev. Lett. **74**, 5144 (1995)
9. Millis, A.J., Shraiman, B.I., Mueller, R.: Phys. Rev. Lett. **77**, 175 (1996)
10. Burgy, J., Mayr, M., Martin-Mayor, V., Moreo, A., Dagotto, E.: Phys. Rev. Lett. **87**, 277202 (2001)
11. Salamon, M.B., Lin, P., Chun, S.H.: Phys. Rev. Lett. **88**, 197203 (2002)
12. Deisenhofer, J., Braak, D., Jug, G., Loidl, A.: Phys. Rev. Lett. **95**, 257202 (2005)
13. Jiang, W.J., Zhou, X.Z., et al.: Phys. Rev. B **76**, 092404 (2007)
14. Jiang, W.J., Zhou, X.Z., Williams, G.: Phys. Rev. B **77**, 064424 (2008)
15. Lu, C.L., Wang, K.F., Dong, S., Wan, J.G., Liu, J.-M., Ren, Z.F.: J. Appl. Lett. **103**, 07F714 (2008)
16. Jiang, W.J., Zhou, X.Z., Williams, G.: Phys. Rev. Lett. **99**, 177203 (2007)
17. He, C., Torijia, M.A., Wu, J., Lynn, J.W., Zheng, H., Mitchell, J.F., Leighton, C.: Phys. Rev. B **76**, 014401 (2007)
18. Souza, J.A., Neumeier, J.J., Yu, Y.-K.: Phys. Rev. B **78**, 014436 (2008)
19. Jiang, W.J., Zhou, X.Z., Williams, G., Mukovskii, Y., Privezentsev, R.: J. Phys. Condens. Matter **21**, 415603 (2009)
20. Tokura, Y., Tomioka, Y., Kuwahara, H., Asamitsu, A., Morimoto, Y., Kasai, M.: J. Appl. Phys. **79**, 5288 (1996)
21. Griffiths, R.B.: Phys. Rev. Lett. **23**, 17 (1969)
22. Bray, A.J.: Phys. Rev. Lett. **59**, 586 (1987)
23. Castro-Neto, A.H., Castilla, G., Jones, B.A.: Phys. Rev. Lett. **81**, 3531 (1998)
24. Burgy, J., Mayr, M., Martin-Mayor, V., Moreo, A., Dagotto, E.: Phys. Rev. Lett. **87**, 2772021 (2001)
25. Zhang, H.G., Li, Q., Liu, H., Chen, L.S., Chen, Y.Y., Li, Y.T.: IEEE Trans. Magn. **46**, 1483 (2010)
26. Salamon, M.B., Chun, S.H.: Phys. Rev. B **68**, 014411 (2003)
27. Zhong, W.J., He, B.: J. Univ. Sci. Tech. China **35**, 328 (2001) (in Chinese)
28. Ivanshin, V.A., Deisenhofer, J., Krug von Nidda, H.-A., et al.: Phys. Rev. B **61**, 6213 (2000)
29. Trukhanov, S.V., Troyanchuk, I.O., Fedotova, V.V., et al..: Phys. Status Solidi (b) **242**, 1123 (2005)
30. Visser, D.W., Ramirez, A.P., Subramanian, M.A.: Phys. Rev. Lett. **78**, 3947 (1997)
31. Lu, W.J., Sun, Y.P., Zhao, B.C., Zhu, X.B., Song, W.H.: Phys. Rev. B **73**, 174425 (2006)
32. Downward, L., Bridges, F., Bushart, S., Neumeier, J.J., Dilley, N., Zhou, L.: Phys. Rev. Lett. **95**, 106401 (2005)
33. Tanaka, J., Nozaki, H., Horiuuchi, S., Tsukioka, M.: J. Phys. Lett. **44**, L129 (1983)
34. He, C., Torija, M.A., Wu, J., Lynn, J.W., Zheng, H., Mitchell, J.F., Leighton, C.: Phys. Rev. B **76**, 014401 (2007)
35. Sarma, D., Rader, O., Kachel, T., Chainani, A., Mathew, M., et al.: Phys. Rev. B **49**, 14238 (1994)
36. Mannella, N., Rosenhahn, A., Watanabe, M., Sell, B., Nambu, A., Ritchey, S., Arenholz, E., Yong, A., Tomioka, Y., Fadley, C.S.: Phys. Rev. B **71**, 125117 (2005)
37. Mannella, N., Rosenhahn, A., Booth, C.H., Marchesini, S., Mun, B.S., Yang, S.-H., Ibrahim, K. Tomioka, Y. Fadley, C.S.: Phys. Rev. Lett. **92**, 166401 (2004)
38. Wang, A., Liu, T., Liu, Y., Cao, G.: Physica B **363**, 115 (2005)
39. Hirota, K., Ishihara, S., et al.: Phys. Rev. B **65**, 064414 (2002)
40. Stern, E.A.: Phys. Rev. B **10**, 3027 (1974)
41. National Institute of Standards and Technology: NIST/FIZ FindIt-code for inorganic crystal structure database (ICSD); ICSD # 50717 is used for $La_{0.7}Sr_{0.3}MnO_3$ (2010)